PHYSICAL REVIEW B VOLUME 50, NUMBER 6 1 AUGUST 1994-II

Distribution of nonequivalent aluminum sites revealed in Al-Cu-Ru and Al-Cu-Fe quasicrystals by ^{27}Al NQR

A. Shastri, F. Borsa,* D. R. Torgeson, and A. I. Goldman
Ames Laboratory and Department of Physics and Astronomy, Iowa State University, Ames, Iowa 50011
(Received 10 May 1994)

The distribution of nonequivalent aluminum sites was studied in Al-Cu-Fe and Al-Cu-Ru stable icosahedral quasicrystalline phases using ^{27}Al NQR spectra taken at 4.2 K. The observed spectra—which give directly the distribution of nonequivalent aluminum sites—were broad, asymmetric, and structureless. A simple electric-field-gradient model calculation accounted for the spectral width in terms of a wide distribution of local atomic environments, and an estimate for the lower limit on the number of nonequivalent aluminum sites was found.

Since their discovery in 1984,[1] quasicrystalline alloys have been studied intensely.[2,3] Although the first examples of aperiodic crystals with icosahedral and decagonal symmetry were metastable phases, stable icosahedral alloys such as Al-Cu-Ru, Al-Cu-Fe, and Al-Pd-Mn have since been discovered and studied.[4] The principal focus of previous work has been a proper description of the atomic-scale structure of quasicrystals. The aperiodicity of these structures precludes a global description of the atomic arrangements in three dimensions, as can be done for periodic crystals. On the other hand, much can be inferred about the structure and physical properties of quasicrystals (QC's) from an understanding of the nature and diversity of local atomic arrangements made possible by probes such as NMR and extended x-ray-absorption fine structure (EXAFS).

NMR and NQR experiments on nuclei carrying a quadrupole moment, eQ, can probe the local electric field gradient (EFG) $V_{ij}^{\rm tot}$ around the resonant nucleus and are thus suitable for studying the distributions of local environments.[5] Previous quadrupole perturbed NMR spectra in powder samples of icosahedral alloys have indicated the presence of a wide distribution of local EFG's at the nuclear site.[6–11] However, no quantitative study could be done mainly because NMR spectra in powders are broadened both by the intrinsic distribution of the local EFG tensor as well as by the distribution of directions of the grains with respect to the external magnetic field. Zero-field NQR experiments, on the other hand, are a direct measurement of the internal local EFG at the nuclear site, since the resonance frequency $\nu_R \propto |V_{zz}^{\rm tot}|$, where $|V_{zz}^{\rm tot}|$ is the largest EFG tensor component in the principal axis system.

We present here an NQR investigation of quasicrystals. A broad ^{27}Al NQR spectrum was found in both Al-Cu-Ru and Al-Cu-Fe stable quasicrystals at 4.2 K. A model calculation of the EFG—using a 1/1 cubic crystalline approximant to the icosahedral phase for calculating the lattice contribution, and using p electrons to calculate the conduction electron contribution—explains the observed NQR spectrum. In particular, the experimental distribution of EFG values can be accounted for by the lattice contribution alone, arising from the distribution of local atomic environments around a given Al site. The continuous distribution of the NQR signal, however, requires many more nonequivalent sites be populated in the icosahedral phase. The EFG model presented here should provide a framework to test cluster decoration models of quasicrystals.

$Al_{70}Cu_{15}Ru_{15}$ and $Al_{65}Cu_{23}Fe_{12}$ alloys were prepared in stable quasicrystalline phases as described previously.[12] All samples were checked with x-ray scans and were found to yield sharp diffraction peaks consistent with the face centered icosahedral phase and with a lack of phason strain. The ^{27}Al NQR and NMR measurements were performed with a phase-coherent pulse Fourier transform spectrometer, and were obtained over a range of frequencies. The ^{27}Al NQR signal was detected at 4.2 K as an echo signal following a $(\pi/2)|_{\{x,\bar{x}\}}-(\pi/2)|_y$ pulse sequence with $\tau_{\pi/2}=10$ μs and pulse separation 100 μs.

The NQR spectra for Al-Cu-Ru and Al-Cu-Fe QC alloys are shown in Fig. 1. The spectra were obtained by plotting the echo intensity vs the frequency of irradiation with proper renormalization for variations of T_2, Q factor, and transmitter power. For ^{27}Al ($I=\frac{5}{2}$) one expects two resonance lines.[5] The $\pm\frac{1}{2}\leftrightarrow\pm\frac{3}{2}$ transition occurs at $\nu_1=\nu_Q g(\eta)$, where $\nu_Q\equiv 3eQ|V_{zz}^{\rm tot}|/20h$, eQ is the nuclear quadrupole moment, and the asymmetry parameter $\eta\equiv(V_{xx}-V_{yy})/V_{zz}$. The function $g(\eta)$ was tabulated in Ref. 13, and varies from 1 for $\eta=0$ to 1.8 for $\eta=1$. The $\pm\frac{3}{2}\leftrightarrow\pm\frac{5}{2}$ transition occurs at $\nu_2=2\nu_Q f(\eta)$, and $f(\eta)$ varies from 1 at $\eta=0$ to 0.88 at $\eta=1$.[13] The echo intensity at the lowest end of the frequency spectrum may have been slightly underestimated as a consequence of the decrease of the power output of the rf power amplifier. The NQR spectrum we report is ascribed to the $\pm\frac{3}{2}\leftrightarrow\pm\frac{5}{2}$ transition of ^{27}Al, and the average ν_R from NQR agreed well with previous quadrupole perturbed NMR spectra in Al-Cu-Fe and Al-Cu-Ru.[11] Due to the extreme width of the NQR spectrum and to the very short $T_2=80$ μs, the signal-to-noise ratio was poor even at 4.2 K. In order to enhance the echo intensity, a weak magnetic field ($H_0\approx 30$ G) was applied by means of Helmholtz coils. The applied field was small enough that it did not affect the shape or width of the NQR spectrum, but was large enough to decouple the nuclear spins, making T_2 longer ($T_2=500$ μs).[14]

The most remarkable feature of the ^{27}Al NQR spectra in Fig. 1 is that the widths are significantly broader than expected from strains, defects, or substitutional impurities, as one can see by comparing with NQR spectra in other sys-

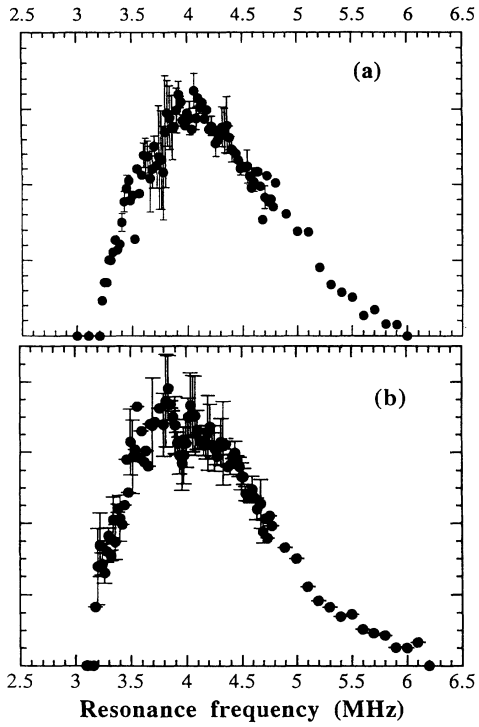

FIG. 1. ^{27}Al NQR spectra for two quasicrystals: (a) $Al_{70}Cu_{15}Ru_{15}$; (b) $Al_{65}Cu_{23}Fe_{12}$ at 4.2 K. Vertical axes were rescaled by ν_R to correct for the Boltzmann distribution.

tems. Since $\nu_R \propto |V_{zz}^{\rm tot}|$—where the proportionality constant depends on properties of the nuclear probe—one should take the ratio of the half width at half maximum σ of the NQR spectrum to the average resonance frequency $\bar{\nu}_R$ to compare quadrupole interactions of different nuclei. For ^{27}Al in Al-Cu-Ru and Al-Cu-Fe quasicrystals we found $\sigma/\bar{\nu}_R \approx \frac{1}{5}$. For alloys where defects and impurities contribute significantly to the NQR linewidth: $\sigma/\bar{\nu}_R = \frac{1}{26}$ for ^{187}Re NQR in rhenium metal,[14] $\sigma/\bar{\nu}_R \approx \frac{1}{79}$ for ^{63}Cu NQR in $YBa_2(Cu_{1-x}M_x)_3O_7$ for a few percent of doping (M=Zn, Ni).[15] A more direct comparison can be made with the ^{27}Al NQR spectrum in $LaAl_2$:Gd (Ref. 16) and UPd_2Al_3,[17] where the zero-field NQR spectra are centered at about 1.5 MHz with a full width of 20 kHz. Also, ^{27}Al NMR spectra in Al-Cu-Fe (Ref. 11) and Al-Cu-Ru (Ref. 18) samples which had received different heat treatments did not show any noticeable differences in the quadrupole interactions, confirming the quadrupole distribution is not controlled by defects. Thus, it seems clear that the large breadth of the observed ^{27}Al NQR spectrum in Al-Cu-Ru and Al-Cu-Fe cannot be attributed simply to the presence of defects in the structure, but rather is the signature of a multiplicity of nonequivalent aluminum sites.

Greater insight into the origin of the broadening of the NQR spectrum may be gained from a model calculation of the EFG distribution for a low-order crystalline approximant to the icosahedral structure. Two equivalent approaches can be used to calculate the EFG in metals.[19] In the first, the crystal is divided into neutral cells centered around each ion, and the EFG at a given nucleus is calculated from the electronic contribution of the central cell, and from the higher-order multiple contributions of the remaining external cells. In the second approach, the EFG is partitioned into a sum of contributions from the bare ionic point charges, and from the conduction or valence electrons. Following the second approach, we write V_{zz} in the principal axis system (PAS) of the EFG tensor, where $|V_{zz}| \geq |V_{yy}| \geq |V_{xx}|$, as[18]

$$V_{zz}^{\rm tot} = V_{zz}^{\rm latt}(1-\gamma_\infty) + V_{zz}^{\rm el}, \tag{1}$$

where the first term is due to the external ionic charges and the second term is due to the valence (or conduction) electrons. The value of $V_{zz}^{\rm latt}$ was calculated in the point charge approximation, and the charge positions were based upon the atomic coordinates of a Al-Cu-Fe(Ru) approximant structure proposed for $Al_{80}Cu_{32}Fe_{16}$.[20] To eliminate boundary effects in the EFG calculation, the original cubic unit cell of 128 atoms and lattice constant $a=12.3$ Å was duplicated and then translated to create a set of 27 identical cells, with the cell of interest at the center. The EFG tensor was then calculated at each Al site in the central cell, summing over ions within a sphere of radius $R<a$, and assuming a particular charge assignment for the Al, Cu, and Fe(Ru) ions. The EFG tensor components were diagonalized to yield the largest component $V_{zz}^{\rm latt}$, $\eta \equiv (V_{xx}^{\rm latt} - V_{yy}^{\rm latt})/V_{zz}^{\rm latt}$, and the angle θ between the z axis of the EFG principal axis system and the z' axis of the unit-cell reference frame defined in the model for the approximant.[20] The results for the distribution of $V_{zz}^{\rm latt}$ and of θ at the different nonequivalent Al sites are shown in Fig. 2. Since the EFG is calculated only out to the fifth nearest-neighbor shell, we estimate an uncertainty in the calculated EFG of about 15% the contribution due to the first coordination shell, the first shell contribution being of order $500e/a^3$. This uncertainty is reflected in the bin sizes of Fig. 2. The distribution of η values, not shown in Fig. 2, ranges from 0 to 1 and has eight different values.

While for Al and Cu it is reasonable to assume the ionic charge which is normally found in the pure metallic phases—i.e., Al^{3+} and Cu^{1+}—the valence assignment for the transition metal ion is uncertain due to the unknown d-shell band structure in the alloy. Thus we performed the calculation for different ionic charges at the Fe(Ru) ion. The overall distribution and mean values of $V_{zz}^{\rm latt}$ are not sensitive to the valence assignment, although the details of the distribution are. In order to simulate the NQR spectrum and obtain agreement with the experiments, it is not unreasonable to assume (i) the two contributions in Eq. (1) have the same PAS, but opposite sign, as is normally found in metals;[19] and (ii) that the average ν_R is primarily due to $V_{zz}^{\rm el}$, which is only weakly site dependent, while the distribution of ν_R comes mainly from $V_{zz}^{\rm latt}$. We write for the Al quadrupole frequency:

$$\nu_R = 2\nu_Q f(\eta) = \frac{3eQ}{10h}[|V_{zz}^{\rm el}| - |V_{zz}^{\rm latt}|(1-\gamma_\infty)] f(\eta). \tag{2}$$

In Eq. (2) we used the values $Q=0.14\times10^{-24}$ cm^2, $(1-\gamma_\infty)=3.3$ for the Sternheimer antishielding factor, and the calculated values of $V_{zz}^{\rm latt}$ and η for the valence assignment Al^{3+}, Cu^{1+}, $Fe(Ru)^{1+}$ to obtain the histogram for the NQR spectrum, which is superimposed on the experimental Al-Cu-Ru NQR spectrum as shown in Fig. 3. The value of $V_{zz}^{\rm el}=1.77\times10^{15}$ esu cm^{-3} was chosen in order to obtain an

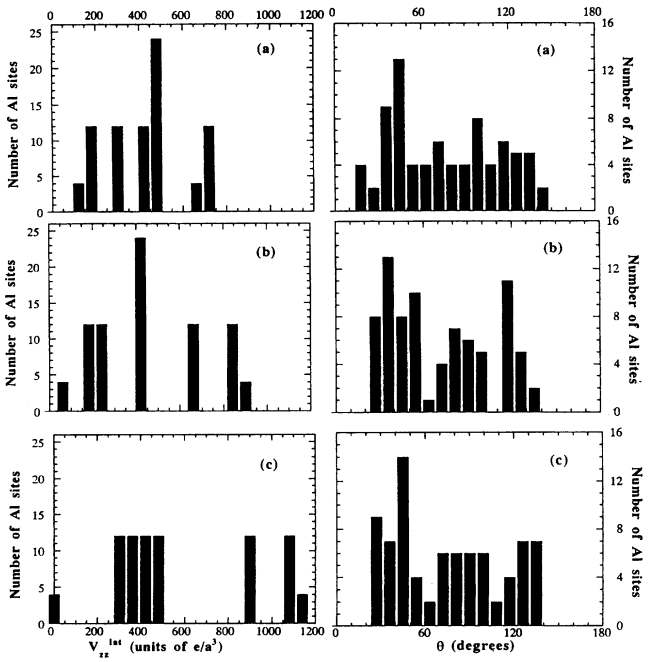

FIG. 2. Histogram of V_{zz}^{latt}—the maximum component of the EFG tensor in its PAS—in units of e/a^3, where $a=12.3$ Å, and histogram of angle θ between the z axis of the PAS and the z' axis of the unit cell. The bin sizes are, respectively, $60e/a^3$ and 9° for the V_{zz}^{latt} and θ histograms, respectively. The Al, Cu, and Fe(Ru) ions were taken, respectively, to have the charges (a) 3,1,1; (b) 3,1,2; (c) 3,1,3.

average ν_R from the histogram which is the same as the experimental value. This value is of the order of magnitude expected for the EFG generated by a $3p$ wave at the Al site. In fact, for a single $3p$ electron in an atom one has[13]

$$V_{zz}^{\text{el}}=(4e/5)\langle 1/r^3\rangle. \tag{3}$$

By using $\langle 1/r^3\rangle=1.28/a_0^3$ ($a_0=0.529$ Å) as obtained from the hyperfine structure of optical spectra of Al neutral atoms[21] one has $V_{zz}^{\text{el}}=3.3\times10^{15}$ esu cm^{-3}. Both the above result and the dominance of the lattice contribution in generating the EFG distribution, which implies weak screening effects, are consistent with the poor metallic character of quasicrystals.

The point-by-point frequency echo intensity spectrum showed no fine structure on a scale of 100 kHz, the resolution limit due to the spectral width of the Hahn echo pulses. Thus we concluded the decoration model for Al-Cu-Fe(Ru) quasicrystals must contain more nonequivalent sites than considered in the approximant used here.

The minimum number of nonequivalent sites was estimated based on reasonable assumptions about the intrinsic linewidth for each nonequivalent site. The intrinsic ^{27}Al dipolar width was estimated[5] to be $2\sigma\approx2$ kHz, and was thus negligible. The inhomogeneous broadening due to defects and strains should be on the order of 20 kHz, based on comparisons with other ^{27}Al NQR linewidths,[16,17] and therefore the small field (30 G) applied to enhance the signal-to-noise ratio could be the major broadening mechanism. Taking an

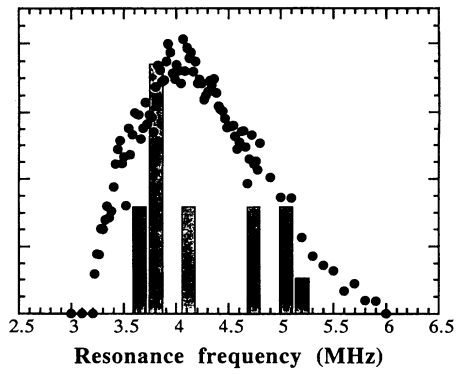

FIG. 3. Comparison of V_{zz}^{latt} histogram for Al, Cu, and Fe(Ru) charges 3,1,1, based on Eq. (2), superimposed on the NQR spectrum for $Al_{70}Cu_{15}Ru_{15}$. The heights of the histogram bars were rescaled to get the maximum of the histogram to agree with the experimental value. The different η values for the nonequivalent sites have been taken into account.

upper limit of 100 kHz for the width of each NQR component broadened by the weak magnetic field,[16] and by dividing the full frequency spread of the NQR spectrum in Fig. 3, i.e., 2.5 MHz, by the half width 50 kHz, we obtained an approximate lower limit of about 50 nonequivalent Al sites.

In order to obtain information about the orientation of the local EFG tensor, we performed an NMR experiment in a single-grain quasicrystal used in a previous study.[22] The results for ^{27}Al NMR in single-grain Al-Pd-Mn QC, which were discussed in detail elsewhere,[18] and obtained by changing the angle α between $\mathbf{H}_0$ and the Al-Pd-Mn single-grain twofold axis, showed a *complete lack* of angular dependence. Furthermore, the NMR spectra in the Al-Pd-Mn single-grain and powder samples *were the same* to within experimental uncertainty. We conclude that the multiplicity of nonequivalent Al sites is characterized by distributions of both magnitudes of the EFG tensor components, and orientations of the PAS. As shown in Fig. 2, the nonequivalent Al sites in the approximant model do indeed display a distribution of orientations of the EFG PAS.

In summary, the NQR signals from icosahedral alloys of Al-Cu-Fe and Al-Cu-Ru showed a broad, continuous character that was consistent with previous NMR studies of the quadrupole distribution in icosahedral alloys. NQR directly probes the distribution of the local EFG at the nuclear sites, and a direct comparison of the NQR spectra with a calculation of the strength and distribution of electric field gradients for a model approximant of the icosahedral phase was presented. The width of the ^{27}Al NQR data was well described by the distribution of quadrupole frequencies calculated using the 1/1 approximant structure and reasonable assumptions about the lattice ionic charges. The agreement between measured and simulated quadrupole resonance frequencies made plausible the conclusion that the measured quadrupole frequencies were largely determined by the electronic contribution to the EFG.

The continuous nature of the distribution, however, requires many more nonequivalent sites than are present in the 1/1 cubic approximant. Our estimates, based upon reasonable values for intrinsic, defect-induced, and instrumental broad-

ening, place a lower limit of about 50 nonequivalent environments for Al. We point out that this number does not necessarily require significant differences in the first- and second-nearest-neighbor shells around Al, since the electric-field-gradient distribution is dominated by the lattice contribution, which is slowly convergent. Indeed, given the good agreement between the width of the NQR resonance and the distribution calculated for the approximant, it is likely that the nearest-neighbor environments are quite similar. The range of non-equivalent local environments in the quasicrystal arises, then, from differences in the third, fourth, or perhaps more distant coordination shells. This implies the structure of the clusters used in the approximant could very well be the same as in the quasicrystal, but that the arrangement of the clusters should be different for the quasicrystal. These differences can effectively broaden the discrete frequencies calculated for the approximant and "fill in" the gaps in the simulated spectrum (see Fig. 3).

The authors thank S. Kycia for the Al-Pd-Mn sample, and S. Qiu for helpful discussions. Ames Laboratory is operated for the U.S. Department of Energy by Iowa State University under Contract No. W-7405-Eng-82.

---

*Also at Dipartimento di Fisica, Universitá di Pavia, 27100 Pavia, Italy.

[1] D. Shectman, I. Blech, D. Gratias, and J. W. Cahn, Phys. Rev. Lett. **53**, 1951 (1984).

[2] A. I. Goldman and M. Widom, Annu. Rev. Phys. Chem. **42**, 685 (1991).

[3] C. Janot, *Quasicrystals: A Primer* (Clarendon, Oxford, 1992).

[4] A. P. Tsai, A. Inoue, and T. Masumoto, Jpn. J. Appl. Phys. **27**, L1587 (1988); A. P. Tsai *et al.*, Philos. Mag. Lett. **62**, 95 (1990).

[5] C. P. Slichter, *Principles of Magnetic Resonance*, 3rd ed. (Springer-Verlag, New York, 1990).

[6] W. W. Warren, H. S. Chen, and J. S. Hauser, Phys. Rev. B **32**, 7614 (1985).

[7] M. Rubinstein and G. H. Stauss, J. Mater. Res. **1**, 243 (1986).

[8] K. R. Carduner, B. H. Suits, J. A. DiVerdi, M. D. Murphy, and D. White, J. Mater. Res. **2**, 431 (1987).

[9] E. Jeong, J. C. Holzer, A. E. Carlsson, M. S. Conradi, P. A. Feddars, and K. F. Kelton, Phys. Rev. B **41**, 1695 (1990).

[10] A. R. Drews, M. Rubinstein, G. H. Stauss, L. H. Bennet, and L. J. Swartzendruber, J. Alloys Comp. **190**, 189 (1993).

[11] A. Shastri, F. Borsa, A. I. Goldman, J. E. Shield, and D. R. Torgeson, J. Non-Cryst. Solids, **153&154**, 347 (1993).

[12] A. I. Goldman, J. E. Shield, C. A. Guryan, and P. W. Stephens, *Proceedings of the 25th Anniversary Adriatico Research Conference on Quasicrystals*, edited by M. Jaric and S. Lundqvist (World Scientific, Singapore, 1990), p. 60.

[13] H. Chihara and N. Nakamura, in *Nuclear Quadrupole Resonance Spectroscopy Data*, edited by K.-H. Hellwege and A. M. Hellwege, Landolt-Boernstein New Series III, **20a**, (Springer-Verlag, Berlin, 1988), pp. 2–37.

[14] C. Dimitropoulos, M. Maglione, and F. Borsa, Phys. Rev. B **37**, 3159 (1988).

[15] K. Ishida *et al.*, J. Phys. Soc. Jpn. **62**, 2803 (1993).

[16] D. E. MacLaughlin and M. Daugherty, Phys. Rev. B **6**, 2502 (1972).

[17] M. Kyogaku, Y. Kitaoka, K. Asayama, C. Geibel, C. Schank, and F. Steglich, J. Phys. Soc. Jpn. **62**, 4016 (1993).

[18] A. Shastri, Ph.D. thesis, Iowa State University, 1994 (unpublished).

[19] E. N. Kaufmann and R. J. Vianden, Rev. Mod. Phys. **51**, 161 (1979).

[20] E. Cocayne *et al.*, J. Non-Cryst. Solids, **153&154**, 140 (1993).

[21] R. G. Barnes and W. V. Smith, Phys. Rev. **93**, 95 (1954).

[22] S. W. Kycia, A. I. Goldman, T. A. Lograsso, D. W. Delaney, D. Black, M. Sutton, E. Dufresne, R. Bruening, and B. Rodricks, Phys. Rev. B **48**, 3544 (1993).

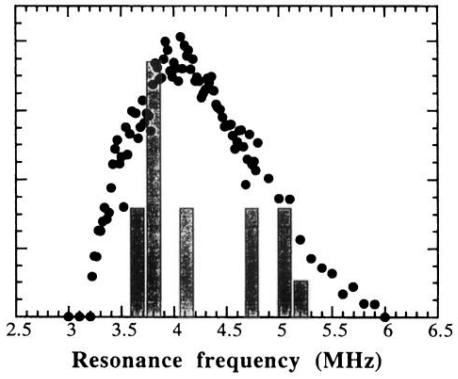

FIG. 3. Comparison of V_{zz}^{latt} histogram for Al, Cu, and Fe(Ru) charges 3,1,1, based on Eq. (2), superimposed on the NQR spectrum for $Al_{70}Cu_{15}Ru_{15}$. The heights of the histogram bars were rescaled to get the maximum of the histogram to agree with the experimental value. The different η values for the nonequivalent sites have been taken into account.